NASA TECHNICAL NOTE

NASA TN D-5836

NASA TN D-5836

PERFORMANCE AND DIAGNOSTICS OF A WATER-COOLED MAGNETOPLASMADYNAMIC ARC THRUSTER

by Denis J. Connolly, Ronald J. Sovie, and George R. Seikel

Lewis Research Center
Cleveland, Ohio 44135

NATIONAL AERONAUTICS AND SPACE ADMINISTRATION • WASHINGTON, D. C. • MAY 1970

1. Report No. NASA TN D-5836	2. Government Accession No.	3. Recipient's Catalog No.
4. Title and Subtitle PERFORMANCE AND DIAGNOSTICS OF A WATER-COOLED MAGNETOPLASMADYNAMIC ARC THRUSTER		5. Report Date May 1970 6. Performing Organization Code
7. Author(s) Denis J. Connolly, Ronald J. Sovie, and George R. Seikel		8. Performing Organization Report No. E-5561
9. Performing Organization Name and Address Lewis Research Center National Aeronautics and Space Administration Cleveland, Ohio 44135		10. Work Unit No. 120-26 11. Contract or Grant No. 13. Type of Report and Period Covered
12. Sponsoring Agency Name and Address National Aeronautics and Space Administration Washington, D.C. 20546		Technical Note 14. Sponsoring Agency Code

15. Supplementary Notes

16. Abstract

The performance of a water-cooled MPD arc thruster using ammonia propellant was studied for a range of operating conditions. Thrust efficiency increased with arc power and with mass flow rate. Thrust efficiency also increased with increasing specific impulse if the specific impulse was raised by increasing the arc power at constant mass flow rate. At constant arc power, thrust efficiency was insensitive to magnetic field strength. The effects of background pressure and magnetic field shape on thruster performance were also studied. By using electrical measurements, such quantities as energy and beam efficiencies, maximum fraction of ionization, and rotating spoke characteristics were determined. By spectroscopic techniques, the composition of the plasma exhaust, the radial and axial profiles of the spectral lines, and the axial velocities of the various species in the exhaust were determined. The variation of all these quantities was studied for a range of thruster operating conditions.

17. Key Words (Suggested by Author(s))	18. Distribution Statement
Water-cooled MPD arc thruster Performance and diagnostics	Unclassified - unlimited

19. Security Classif. (of this report)	20. Security Classif. (of this page)	21. No. of Pages	22. Price*
Unclassified	Unclassified	39	$3.00

*For sale by the Clearinghouse for Federal Scientific and Technical Information
Springfield, Virginia 22151

PERFORMANCE AND DIAGNOSTICS OF A WATER-COOLED MAGNETOPLASMADYNAMIC ARC THRUSTER

by Denis J. Connolly, Ronald J. Sovie, and George R. Seikel

Lewis Research Center

SUMMARY

The performance of a water-cooled magnetoplasmadynamic (MPD) arc thruster using ammonia propellant was studied for a range of operating conditions. Thrust efficiency increased with arc power and with mass flow rate. Thrust efficiency also increased with increasing specific impulse if the specific impulse was raised by increasing the arc power at constant mass flow rate. At constant arc power, the thrust efficiency was insensitive to magnetic field strength.

The effects of background pressure and magnetic field shape on thruster performance were also studied. By using electrical measurements, such quantities as energy and beam efficiencies, maximum fraction of ionization, and rotating spoke characteristics were determined. By spectroscopic techniques, the composition of the plasma exhaust, the radial and axial profiles of the spectral lines, and the axial velocities of the various species in the exhaust were determined. The variation of all these quantities was studied for a range of thruster operating conditions.

INTRODUCTION

In recent years, the magnetoplasmadynamic (MPD) arc thruster has received considerable attention as a possible competitor to ion thrusters for future electric propulsion applications. A potential advantage of MPD thrusters is that they may be able to operate directly from low-voltage power sources. Some of the power conditioning equipment necessary for ion thrusters would therefore be eliminated. At most, the MPD arc thruster requires two sources of low-voltage direct-current power, one for the arc and one for the magnet. It is possible that solar-cell panels could supply the power directly with no power conditioning. One of the power supplies could be eliminated if the magnetic field were supplied by permanent magnets or by an electromagnet in series with the arc.

A study of permanent-magnet designs for radiation-cooled thrusters (ref. 1) showed that the optimum magnet design (the lightest magnet for a given field intensity) produced a fairly divergent magnetic field. Consequently, a knowledge of the effect of field shape on thruster performance is necessary to determine the feasibility of using permanent magnets.

This report presents the results of a number of experimental studies on MPD arc thruster performance (refs. 2 to 5). All experiments were performed in a large, high pumping capacity, vacuum facility. Special studies were made to determine the effects of magnetic field and background pressure on thruster performance. The thruster efficiency was mapped for a wide range of operating parameters. Finally, a number of electrical and spectroscopic diagnostic studies were aimed at increased understanding of the MPD arc thruster.

APPARATUS AND MEASUREMENT TECHNIQUES

All experiments were performed in a 4.6-meter-diameter, 19.8-meter-long vacuum tank (ref. 6). The experiments were performed using the water-cooled MPD arc thruster shown in figure 1 and described in references 7 and 8. This thruster has two axial magnetic field coils. One coil is located upstream, and one downstream, of the cathode tip. The divergence of the thruster magnetic field can be varied by varying the ratio of the currents in the two coils.

Thrust and Mass Flow Rate Measurements

The thrust measurements were made using a parallelogram-pendulum thrust stand. The electrical power for the thruster and magnet coils was brought onto the stand through coaxial lines that terminated in coaxial mercury pots. The power was supplied by commercially available welding power supplies. Deflection of the stand was sensed by a linear differential transformer, with output indicated on a strip-chart recorder. The thrust stand was calibrated by a weight-and-pulley arrangement, which was used to apply known forces to the stand. A 25-centimeter-diameter steel bucket, or "thrust killer," was mounted on a shaft on the thrust stand and could be swung down in front of the thruster to remove the directed energy of the beam. The thrust was measured by blocking the exhaust beam momentarily with the thrust killer and observing the change in thrust stand deflection.

As a check on the thrust killer technique, the stand deflection resulting from turning off the arc current was measured at a number of operating points. This thrust value

was corrected for current tare (obtained by shorting anode to cathode) and cold-flow tare. Comparison of these results with the corresponding thrust killer measurement produced agreement within 5 percent. Gaseous propellant flow rates were measured by the use of small, jeweled, sonic orifices calibrated for flow rate against upstream pressure.

Calorimetric Measurements

Cooling-water flow rates were metered by the use of turbine flowmeters. The inlet and outlet temperatures of the cooling circuits were measured by using thermocouples. Power removed by the anode, cathode, and magnet cooling circuits was calculated by using the product of the appropriate flow rate and temperature rise. The turbine flowmeters are quite accurate, contributing an error of under 1 percent. For a variety of reasons, however, we expect our measured temperature rises (final temperature minus initial temperature) to be in error by as much as 10 percent. The power loss measurements are therefore accurate to within about 10 percent. The greater part of this error is systematic, being due to variations in thermocouple properties and nonoptimum thermocouple placement. The nonsystematic part of the error is smaller, being typically 2 or 3 percent. Changes in power losses due to changes in thruster operating conditions are therefore measured well within 5 percent.

Background Pressure Measurements

At pressures below 10^{-3} torr the tank pressure was measured by a Bayard-Alpert-type ionization gage. Above 10^{-3} torr a thermocouple gage was used. Both gages were calibrated by using air. A correction factor is conventionally applied for other gases, but in many of our experiments the tank contained a mixture of two or more gases in unknown ratios. For this reason, correction factors were not applied to the gage readings. Pressures quoted should be considered accurate within about a factor of 2.

Spectroscopic Measurements

All spectroscopic data were obtained by using an 0.5-meter Ebert scanning monochromator with photoelectric readout. The optical system was calibrated by using a standard tungsten ribbon filament lamp calibrated by the National Bureau of Standards. Initial spectroscopic data were obtained from a side view of the exhaust beam at points from 0.5 to 4.5 centimeters downstream of the exit plane of the anode. By using a

mirror and lens system, a section of the beam 10 centimeters high and 5 to 20 micrometers in width was observed. Initial spectroscopic data were all obtained with the thruster operating on ammonia (NH_3).

In order to study the variation in plasma composition with thruster operating parameters, a series of identification spectra was taken. These spectra were analyzed and certain sensitive lines for each element observed were chosen. The intensities of these lines were then monitored as the thruster was run over a wide range of operating conditions. The spectral lines monitored for each element are given in table I. The 3360- to 3370-Å region was also monitored in order to detect the presence of NH, but it was not observed during this series of experiments.

The axial velocities were obtained by measuring the Doppler shifts of the various spectral lines emitted by the plasma constituents. The measurements were made by using the same 0.5-meter Ebert monochromator with a somewhat more complicated optical system. This optical arrangement is shown in figure 2.

Light from the beam goes into the monochromator by two paths. The unshifted, or reference, light is obtained by viewing the plasma perpendicular to the flow direction. The Doppler-shifted light is obtained by viewing the plasma at angles varying from 45° to 53° to the flow direction. The lenses L_1 and L_2 image the plasma beam on the entrance slit of the monochromator. Measurements are made at various axial positions by moving the image across the slit by rotating mirror M_4. Of course, this necessitates a correction for the change in viewing angle.

The fact that the perpendicular viewing did give unshifted wavelengths was verified at several axial positions by comparing wavelengths with a standard light source.

The resolution of the monochromator was about 0.2 Å. In addition, the lines were quite broad because of the rotational and thermal motion of the plasma. Therefore, the peaks of the shifted and unshifted light would overlap if viewed simultaneously. This problem is avoided by the use of a chopping procedure. By alternately chopping one light path and then the other, separate traces are obtained for the two lines during a single scan.

The degree of accuracy and resolution obtained by using this chopping technique was determined by calibrating the system with standard light sources. In the calibration procedure, the standard light sources are put in each optical arm. The traces obtained using H_2 and Ar lamps are shown in figure 3. The upper solid trace is that obtained for H_2 and Ar together, and the lower trace is for H_2 and Ar chopped. In the chopped trace, the solid portions were obtained from the photomultiplier output. The dashes that fill in the line shapes were obtained by fitting the chopped data over the profiles obtained when either H_2 or Ar only was used. By using this technique, the individual line shapes could be reproduced exactly, and wavelength separations as low as 0.08 to 0.1 Å were measured with 10 percent accuracy. This would correspond to an uncertainty in velocity of about 1000 meters per second.

In the case illustrated, we chopped five times while scanning through the line. Because of the reproducibility of the line shapes this usually was unnecessary. In some cases, namely for shifts greater than about 0.15 Å, only a single chop was needed. That is, the shifted light was blocked until we scanned past the peak of the reference line. We then switched to the shifted line and recorded the remainder of it, including the peak. Some examples of these traces are shown in figures 4(a) to (c).

Beam Current Density Measurements

The beam of the water-cooled thruster was probed with small toroidal current detectors (i.e., Rogowski coils). The Rogowski coil system could measure alternating currents threading it with frequencies between 10 kilohertz and 10 megahertz. The Rogowski coils consisted of approximately 400 turns in two layers with a toroidal minor diameter of 0.5 centimeter and a toroidal major diameter of 1.9 centimeters. The coils were mounted on a pendulum which carried them through the thruster beam. A pair of contacts, one on the pendulum and one on the thrust stand support, was arranged to provide a trigger signal when the coil crossed the vertical center plane of the beam. The path of the coil through the beam was chosen to pass 0.6 centimeter above the axis of the thruster and 1 centimeter downstream of the exit plane of the nozzle (see fig. 1). In the case of double-coil tests, the second coil was mounted on the pendulum 1.2 centimeters below the first in order that the two coils would be diametrically across the beam at the time the signals were recorded. The coil output was amplified and integrated by commercially available oscilloscope plug-in preamplifiers and fed to an oscilloscope which was triggered when the coil was in the center of the beam. The fundamental frequency of the current linking the coil was obtained from the oscilloscope photographs. To ensure that the measured output was due to a current linking the coil, a number of runs were made with the hole in the torus blocked by a strip of mica and no signal was noted. When the pair of coils was swung through points diametrically across the beam, a 180° phase relation between the two signals was obtained, indicating that the oscillating current was of a rotational nature. In some cases, an oscilloscope across the thruster electrodes was triggered at the same time as the Rogowski coil readout. The arc also caused small amplitude fluctuations of the same frequency to be induced in the arc voltage.

Obtaining the frequency of rotation from oscilloscope photographs was both tedious and inaccurate. Consequently, a more suitable arrangement was used in surveying the dependence of frequency on thruster operating conditions. A thin flat coil of 100 10-centimeter-diameter turns was placed in proximity to the thruster. The voltage induced in the coil due to the periodically varying current direction was amplified, and the frequency metered by use of an electronic counter.

THRUSTER PERFORMANCE

Measurements were made of thrust, arc current, arc voltage, and propellant flow rate. These parameters were then used to calculate specific impulse and thrust efficiency given, respectively, by

$$I_{sp} = \frac{T}{\dot{m}g} \tag{1}$$

$$\eta_T = \frac{T^2}{2\dot{m}P_a} \tag{2}$$

where T is the thrust, $\dot{m}$ the mass flow rate, g the gravitational constant, and P_a the power supplied to the arc. The efficiency η_T is only an arc efficiency (i.e., it does not include magnet power).

All the data reported herein, with the exception of some special spectroscopic studies, were taken while operating the water-cooled thruster with ammonia propellant. The magnetic field at the cathode tip was varied from 0.06 to 0.14 tesla. The propellant flow rate was varied from 0.02 to 0.19 gram per second. The tank pressure varied from 4×10^{-5} to 2×10^{-4} torr, depending on propellant flow rate. In all runs on the water-cooled thruster, the power removed by anode and cathode cooling water was calculated, as previously described, from measured flow rates and temperature rises. This power P_{cw} was then used to calculate an energy efficiency η_e given by

$$\eta_e = \frac{P_p}{P_a} = \frac{P_a - P_{cw}}{P_a} \tag{3}$$

where P_p is the net power coupled to the plasma. For comparison with spectroscopic data, a "beam efficiency" was also calculated by

$$\eta_b = \frac{T^2}{2\dot{m}P_p} = \frac{\eta_T}{\eta_e} \tag{4}$$

The energy efficiency is thus the efficiency of transferring electrical power to the gas, while the beam efficiency is the efficiency of converting this power into useful thrust.

Figure 5 shows thruster performance data. These data were taken at mass flow rates of 0.03 to 0.19 gram per second, tank pressures of 2×10^{-4} to 4×10^{-4} torr and magnetic fields from 0.07 to 0.14 tesla. The arc power varied from about 10 to 80 kilowatts for this range of parameters. The thrust efficiency at a given arc power was found to be insensitive to magnetic field. It is clear from figure 5, however, that the ammonia

performance does depend on mass flow rate. The thrust efficiency at a given specific impulse increases with increasing mass flow rate. An increase in arc power is required to increase either flow rate at constant specific impulse or specific impulse at constant flow rate. Hence, thrust efficiency always increases with increasing arc power.

Thruster Voltage-Current Characteristics

It has been pointed out previously (refs. 8 and 9) that MPD thrusters operating with ammonia tend to run in either a high-voltage mode (HVM) or a low-voltage mode (LVM). In describing our experiments, however, it is necessary to discuss at least three different voltage modes: low, high, and medium voltage. At low flow rates (0.01 to 0.03 g/sec) and low magnetic fields (0.06 or 0.07 T), the two-mode behavior was most evident. The arc ran either in a high-voltage mode of 60 to 75 volts or in a low-voltage mode of 30 to 40 volts. In these cases, the arc could be changed from one mode to the other rather easily. Increasing the current above a certain value (dependent on magnetic field and mass flow rate) caused the arc to jump from the high- to the low-voltage mode. Decreasing the current below some other value caused a jump back to the high-voltage mode. The stable current ranges sometimes did not overlap.

On other occasions, the arc operated stably in a medium-voltage mode (MVM) somewhere between 40 and 60 volts. This situation usually prevailed at higher mass flow rates (above 0.04 g/sec) or higher magnetic field (above 0.1 T). Typical voltage-current curves for the three modes are shown in figure 6(a). In all cases, the voltage increased with increasing magnetic field strength. A sample of the variation in arc voltage for various magnetic field strengths is shown in figure 6(b).

Energy Losses

In order to estimate the relative importance of various power losses, the ammonia propellant beam efficiency was compared with calculated values of a frozen-flow efficiency η_f. This theoretical efficiency is obtained by assuming that the only energy lost in the plasma is that required for ionization. That is, the power coupled to the plasma P_p is either converted to thrust or used to ionize the propellant.

The frozen-flow efficiency can be simply related to the fraction of ionization and is given by the following expression:

$$\eta_f = \frac{P_T}{P_T + P_{ion}} = \frac{\frac{T^2}{2\dot{m}}}{\frac{T^2}{2\dot{m}} + aK\dot{N}} \tag{5}$$

where P_T and P_{ion} are thrust power and ionization power, respectively, a is the degree of ionization, K the energy cost per molecule ionized, and $\dot{N}$ the flow rate in molecules per second. Equation (1) can be used to express equation (5) more conveniently as

$$\eta_f = \frac{I_{sp}^2}{I_{sp}^2 + \frac{2aK}{Mg^2}} \tag{6}$$

where M is the mass of an ammonia molecule. Considering no energy losses other than dissociation and ionization potentials, the reaction
$NH_3 \rightarrow N^+ + 3H + e \rightarrow N^+ + 3H^+ + 4e$ will require about 70 electron volts. Due to atomic radiation, the minimum energy cost per ion is usually about twice the ionization potential at electron temperature, ≥5 electron volts in the optically thin case (refs. 10 and 11). Consequently, an energy cost of 140 electron volts was assumed to fully dissociate and ionize each NH_3 molecule.

The experimentally determined beam efficiency η_b is the ratio of the power converted into thrust to the net power coupled to the plasma. This measurement takes into account both ionization losses and unrecovered thermal and kinetic (i.e., swirl) energy in the beam. Consequently, η_b will always be smaller than η_f. However, the experimental η_b values can be compared with the calculated frozen-flow efficiencies in order to estimate the maximum possible degree of ionization in the plasma.

The maximum possible fraction of ionization is calculated by substituting η_b for η_f in equation (6). The result is plotted against specific impulse in figure 7 for two different mass flow rates, 0.02 and 0.06 gram per second.

From figure 7, a number of things are clear. First, the maximum possible fraction of ionization increases with increasing specific impulse. It also increases with decreasing mass flow rate at constant specific impulse. In the 0.06-gram-per-second data, the maximum calculated fraction of ionization never exceeds about 30 percent. The MPD thruster, therefore, is clearly able to accelerate a partially ionized beam. Consequently, the thruster efficiency is not limited by the fully ionized frozen-flow efficiency of the propellant used.

From figure 7, the maximum possible fraction of ionization is less when operating at higher mass flow rate. It might be expected, therefore, that the improvement in per-

formance with increasing flow rate is due to improved beam efficiency. Figure 8, however, shows that this is only part of the story. For most of the specific-impulse range, both beam efficiency and energy efficiency improve with increasing mass flow rate. Both, therefore, contribute to the improvement in thrust efficiency at constant I_{sp}.

At constant mass flow rate, however, only the beam efficiency improves significantly with specific impulse. The increase in thrust efficiency with increasing specific impulse at constant mass flow rate is therefore due entirely to an increase in beam efficiency.

Effect of Magnetic Field Shape on Thruster Performance

The optimum permanent-magnet design for MPD thrusters produces a fairly divergent magnetic field (ref. 1). That is, the axial field decreases downstream of the cathode tip. We therefore performed a series of experiments to determine if this field divergence is detrimental to thruster performance. The shape of the magnetic field at the cathode tip can be varied by changing the currents in the two electromagnets shown in figure 1. The axial magnetic field produced by the two thruster coils can then be calculated as a function of the two currents. In the calculation, the coils were approximated as current loops. Gaussmeter measurements made at various positions were found to agree with the calculated values to within 4 percent. The expression for magnetic field B was then differentiated with respect to the axial coordinate z in order to obtain the field-shape parameter $(1/B_z)(\partial B_z/\partial z)$. This quantity is the logarithmic derivative of the axial field evaluated at the cathode tip. The field-shape parameter was varied by varying the ratio of the currents in the two coils. The effects of the magnetic field shape on thruster performance are shown in figure 9. The thrust-to-arc-power ratio is plotted against field-shape parameter for a number of operating conditions. For each curve, the mass flow rate was held constant. The arc power and magnetic field strength at the cathode tip were also held approximately constant (within about ±5 percent). The thrust was measured for each setting of the field-shape parameter.

Figure 9 shows that the thruster performance is not strongly affected by field shape for field-shape parameters in the range +0.1 to -0.2 cm^{-1}. Optimum lightweight permanent magnets can be designed to have field divergences in this range (ref. 1). It is therefore concluded that permanent magnets could be used in MPD arc thrusters without lowering the thruster performance. The field divergence was varied for the $\dot{m}$ = 0.03 gram per second case until a definite effect was noticed. It was found that thruster performance was seriously degraded at a field-shape parameter of -0.4 cm^{-1}.

Studies of Background Pressure Effect

In studying the effect of background pressure on thruster operation, the tank pressure was varied in one of two ways. In some cases, the thruster was started at an intermediate pressure (~ 0.5 torr) and data were taken while the tank pressure was being reduced to its ultimate value (5×10^{-5} to 5×10^{-4} torr depending upon $\dot{m}$). In other cases, a controlled flow of inert gas was bled into the tank with the pumping system fully operational. In the latter cases, the bleed gas was never the same as the propellant, ammonia or hydrogen. The bleed gas was usually nitrogen when hydrogen was the propellant, and argon when ammonia was the propellant.

The former method of varying tank pressure more nearly simulated the experiments of others. The latter method had two important advantages:

(1) The tank pressure could be set and maintained indefinitely at any value in the range of interest.

(2) The propellant and background particles could be spectroscopically discriminated from each other. As a result, the behavior of the beam gas and the background gas could be independently studied as the pressure was varied.

Data were taken by both methods. The thrust was measured as a function of tank pressure while holding arc power and mass flow rate approximately constant. For a number of conditions, the thruster beam was studied spectroscopically. Relative intensity of emission from the background gas was measured. These measurements were used as one criterion of the effect of this gas on thruster operation. Axial velocity of both propellant gas and background gas was measured by the Doppler-shift technique described previously.

There has been a great deal of doubt concerning the effect of background gas on MPD thruster operation (ref. 12). The available data on the subject (refs. 8, 13, and 14) lead to no conclusion and even seem contradictory. In the results of Jones and Walker (ref. 8), the thrust decreased monotonically with increasing tank pressure. In the results of Cann, et al. (refs. 13 and 14), there is a minimum in the thrust-against-tank-pressure curves. And the overall thrust was higher at the high pressures than that obtained at the lowest pressure attainable. We have observed both types of results. In figure 10, the thrust-power ratio is plotted against tank pressure for ammonia propellant at three different mass flow rates. At the highest mass flow rate (0.06 g/sec), the thrust-power ratio decreased monotonically with increasing tank pressure in agreement with the results of Jones and Walker (ref. 8). At the lowest mass flow rate, the thrust-power ratio at first decreased then increased with increasing tank pressure. In general, however, the thrust-power ratio had its maximum value at minimum tank pressure. This is in qualitative agreement with the results of reference 8.

In obtaining the data of figure 10, the tank pressure was varied by varying the pumping capacity while operating the thruster. Thus, the background gas was the same gas

as the propellant. The results of reference 8 were obtained either by varying the pumping capacity or by bleeding hydrogen into the tank while operating on hydrogen. Again, the background gas was the same as the propellant.

For the data shown in figure 11, the tank pressure was varied by bleeding nitrogen into the tank while the thruster was operating on ammonia or hydrogen. Again, at high mass flow rate, the thrust-power ratio fell off monotonically with increasing tank pressure. At intermediate mass flow rate, there is a pronounced minimum in the curve at a pressure of about 0.01 torr. This case is quite similar to the general behavior of Cann's data (ref. 14), the minimum even occurring at about the same pressure. Finally, at a very low mass flow rate, there is a steep rise in the thrust-power ratio as the pressure is increased above about 0.01 torr. In all of Cann's data, as in the data of figure 11, the tank pressure was varied by bleeding a gas, other than the propellant, into the vacuum tank. In our tests, this method was common to all the cases in which a pronounced minimum occurred in the curve of thrust-power ratio against tank pressure, or in which the maximum thrust occurred at pressure other than the minimum.

Of course, interest in the effect of environmental pressure stems primarily from the limitations of most available vacuum facilities. Those who must take measurements on a thruster operating in a high-background-pressure environment (~ 0.1 torr) need some basis for estimating the effect of the background gas on their results. For this purpose, the results of figure 10 are appropriate. In figure 10, the thrust decreases monotonically with increasing tank pressure except for the low-mass-flow-rate case (0.005 g/sec). Even in this case, the thrust at the highest pressure studied did not exceed that measured at the minimum tank pressure. The thruster will not run at low background pressure with mass flow rates lower than 0.005 gram per second, although it will run at higher pressure. It thus appears that for these low flow rates ($\dot{m} \leq 0.005$ g/sec) the presence of the background gas augments the measured thrust. Otherwise, the background gas usually causes a decrease in measured thrust. What constitutes a low flow rate in this context depends upon the thruster under study. We know of no way to determine this range from measurements made at high tank pressures.

There is a further point of interest in the data of figures 10 and 11. In both cases, but especially in figure 11, the curves tend to converge at high tank pressure, obscuring the dependence of thrust on mass flow rate. This implies that the fundamental phenomena of thruster operation may be considerably different at high pressure than at low pressure. The applicability of diagnostic measurements made at high tank pressure may therefore be questionable.

In the above discussion, we have tacitly assumed that our lowest achievable background pressures (10^{-5} to 10^{-4} torr) are adequate to eliminate the effect of background gas on thruster operation. There is a certain amount of experimental evidence to support this assumption. Figure 12 is a plot of thrust-power ratio against tank pressure for a water-cooled thruster operating on ammonia. The arc power was 25 kilowatts, and

the mass flow rate was 0.020 gram per second. The background pressure was varied by bleeding argon gas into the tank. The data show little effect of background pressure below 0.01 torr. The average axial velocity of the singly ionized nitrogen (4630.6 Å) in the thruster exhaust was measured at a number of axial positions. The measurements were performed with the Doppler-shift technique described previously. For the four tank pressures indicated by arrows in figure 12, the axial velocity is plotted against axial position in figure 13. Figure 13 shows that for these pressures the velocities are the same. That is, to a tank pressure of 10^{-3} torr, the velocity of the ions in the thruster exhaust is insensitive to the presence of the argon. In addition, at each of the above pressures, the argon spectrum lines were not intense enough to be separated from the weak background spectra of molecular hydrogen and nitrogen. That is, argon spectrum lines were about 2 orders of magnitude lower in intensity than the N^+, N^{++}, and H lines. It thus appears that there are no background pressure effects on thruster operation for these pressures. At higher tank pressures (>0.01 torr), the N^+ velocity began to decrease and argon lines became intense enough to be positively identified. At a pressure of 0.2 torr the N^+ velocity was greatly reduced. In addition, the argon ion line used (4589.9 Å) began to exhibit a Doppler shift. The N^+ and A^+ velocities obtained at 0.2-torr tank pressure are also shown in figure 13. (It should be pointed out that at these low velocities the uncertainty in the measurement can approach a factor of 2.) At 0.2 torr, the argon lines were comparable in intensity to the nitrogen lines. The relative line intensities depend on many factors besides the relative abundance of each species. Not all these factors are known. Hence, it is not possible to say whether there is enough argon moving to account for the increase in thrust as well as to compensate for the decrease in velocity of the primary propellant. The results of figure 13 do, however, indicate three things:

(1) The argon background gas has no significant effect on thruster operation at pressures below about 10^{-3} torr.

(2) At higher pressures, the argon background gas reduces the exit velocity of the primary propellant.

(3) At higher background pressures, the argon is entrained and accelerated by the thruster.

Similar conclusions can be drawn from figures 14 to 16. Figure 14 shows thrust-power ratio against tank pressure for hydrogen propellant and nitrogen background gas. The hydrogen mass flow rate is 0.0035 gram per second, and the arc power is about 20 kilowatts. Spectroscopic data were taken at the five different pressures indicated by the arrows on figure 14. Note that thrust-power ratio is approximately constant at the five pressures. In figure 15, the axial velocity of the neutral hydrogen atom (4861.3 Å) and the singly ionized nitrogen atom (4630.6 Å) are plotted against axial position for these pressures. In figure 16, N^+ intensity is plotted against position for the three highest of the five pressures. At tank pressures of 3×10^{-5} and 2×10^{-4} torr, the velocity

falls on the same curve. The nitrogen line was not observed at these pressures. At 8×10^{-4} torr, the axial velocity decreased as shown. Also at 8×10^{-4} torr, the nitrogen line appeared with a Doppler shift. With each succeeding increase in pressure, there was a substantial drop in axial velocity of the hydrogen atom. Also with each succeeding increase in pressure, there was a large increase in the intensity of the nitrogen line with only modest changes in the velocity associated with the nitrogen line. The velocity-intensity product of the nitrogen line should be a crude, but meaningful, indicator of the momentum flux of the nitrogen entrained into the beam. It can be seen by inspection of figures 15 and 16 that this product increases rapidly with increasing tank pressure. Taken together, the data of figures 15 and 16 indicate that, at pressures well below 10^{-3} torr, the thruster operation is not significantly influenced by the presence of the background gas. At pressures near and above 10^{-3} torr, the background gas is again found to have a dual effect on thruster operation. The exit velocity of the primary propellant is reduced, and the background gas is entrained and accelerated. The first effect reduces the measured thrust, while the latter increases it. Over a wide range in pressure, the two effects on thrust appear to just about balance in the present case. Also, in the present case the latter effect appears to eventually dominate. In the general case, both effects increase with increasing pressure. The relative importance of the two effects depends on mass flow rate with entrainment being relatively less important at higher mass flow rates.

SPECTROSCOPIC OBSERVATIONS

Spatial Variation of Spectra

Radial variation of the spectral line intensities were obtained at axial positions 0.5, 1.5, and 4.5 centimeters downstream of the anode exit plane. These variations are shown in figure 17 for the 0.5-centimeter position. The intensities have been normalized to 1 at their maximum value. The general appearance of the plasma beam is the same as has been described previously; that is, there is an intense central core which is surrounded by a region of lower intensity. The profiles for N^+, N^{++}, H, and N_2 only are shown on figure 17. The H_2 profile (not shown) essentially follows the H profile and the N_2^+ profile is essentially the same as the N_2 profile. Figure 17 shows that the N^+ and N^{++} species are confined to the hot central portion of the beam. Furthermore, the flat peaks exhibited by the N_2 and N_2^+ profiles seem to indicate that there is a hole in the center of the radial density profile for these species. Not surprisingly, the profile for each of the elements becomes broader downstream. The variation in intensity of the observed spectral lines with axial position, again normalized to 1, is shown in figure 18.

Besides these purely qualitative data, attempts were made to obtain quantitative

spectroscopic data. The plasma was seeded with helium in an attempt to determine the type of plasma being observed (i.e., equilibrium, tenous, etc.) and to measure the electron temperature and degree of ionization by using the methods described in references 15 and 16. However, the helium lines were masked by the great number of lines in the ammonia spectrum.

In general, although ammonia is a relatively attractive propellant from a performance standpoint, it leaves much to be desired in terms of ease of diagnostics. The complex kinetics of electron-ammonia interactions and the spectroscopic invisibility of the hydrogen ion are two conspicuous difficulties. Operation of the thruster on a heavy inert gas for spectroscopic diagnostics would substantially simplify the study of plasma properties.

Axial Velocity of Thruster Exhaust Species

A spectroscopic measurement of interest which is feasible with ammonia propellant is the Doppler shift caused by axial velocity. Although the spectroscopically invisible hydrogen ion is still present, most of the momentum flux in the beam is carried by heavier visible particles.

In order to obtain the axial velocity component from Doppler shifts, we must ensure that there is no net time average shift as a result of azimuthal plasma rotation or asymmetries. Radial profiles of the spectral lines (fig. 17) taken in the perpendicular arm (fig. 2) show that the intensities peak sharply at the plasma centerline. The rotational velocities at the centerline are perpendicular to the viewing direction. Consequently, the perpendicular viewing should produce a spectral line broadened about an unshifted peak. The same argument (relative to rotational velocities) applies when the plasma is viewed at 45° to the flow direction. The fact that the perpendicular viewing did give unshifted wavelengths was verified at several axial positions by comparing wavelengths with a standard light source. Such measurements also rule out any shifts in the line peaks caused by Stark or Zeeman effects.

The Doppler-shift results represent an average velocity along the viewing path. There is consequently an uncertainty in the axial position since the plasma is viewed at 45° to its direction of propagation. The spectral intensities peak at the beam center, and we consider the axial resolution to be plus or minus the radial distance required for the line intensity to be one-half that at the beam center. By this criterion, the axial resolution for N^{+} and N^{++} varies from ± 0.5 centimeter at the anode exit to about ± 0.9 centimeter further downstream. That for the neutrals varies from ± 0.75 to ± 1.5 centimeter. The points on the figures 13, 15, 16, 19, and 20 represent the intersection of the beam axis and the viewing line.

Typical results for the velocity of the various exhaust species are illustrated in fig-

ure 19. The plot shows the axial velocity against axial distance from the anode exit plane. For this data and all other cases examined, acceleration of both the ions and neutrals always occurred outside the thruster. This clearly demonstrates the action of the magnetic nozzle. The N^+ and N^{++} ions reached about the same peak velocity. This velocity was always greater than the value calculated by $T/\dot{m}$. Fast neutrals were observed in every run but their velocities were always lower than those of the ions. The observed neutral velocities were about equal to $T/\dot{m}$. Increasing the arc power and mass flow rate such that I_{sp} was kept constant left the velocities relatively unchanged (fig. 20(a)). Increasing the arc power at constant $\dot{m}$ (figs. 20(b) and (c)) results in higher ion and neutral velocities.

From the above discussion, the average axial velocity of all the particles observed must be higher than the measured $T/\dot{m}$. This, however, is to be expected. Most of the light comes from the electron-rich core of the beam. The particles in this region would certainly have higher axial velocity, if not higher overall velocity, than the average of those in the thruster exhaust.

The high axial velocity of the neutrals dovetails nicely with our earlier conclusion that the MPD thruster can accelerate a partly ionized gas. Taken alone, the Doppler-shift measurements do not require this conclusion. The fast neutrals could be recombined ions, but the data of figures 7 and 8 rule this out. The gas was simply not supplied with enough energy to fully ionize it.

An acceleration voltage can be defined from the maximum measured ion velocities by using the relation $m_i v_m^2/2 = qVi$, where m_i is ion mass, v_m is maximum velocity, and V_i is acceleration voltage. The V_i calculated from the peak ion velocities are often much higher than the arc voltage; no correlation was found between arc voltage and V_i.

The variation of ion velocity with magnetic field shape was also investigated. For the same operating conditions, the ions reached essentially the same peak velocities. However, as the divergency of the field lines was increased at the cathode tip, the ions reached these peak velocities closer to the anode exit plane.

Comparison of Axial Velocity Measurements with the Results of Others

We cannot, at present, make a complete and meaningful comparison of our Doppler-shift studies with the results of others. The earliest Doppler-shift studies of MPD thruster beams were reported by Bohn, et al. (ref. 17), and Jacobs, et al. (ref. 18). Bohn studied the radial variation of the axial velocity in an argon arcjet. Unfortunately, his studies were made at a single axial position and a high background pressure, and his results were strongly affected by the entrainment of background gas (private communication from W. L. Bohn). Jacobs studied a lithium MPD arcjet at angles of from 8^o to

10^{o} from the axis of the beam. Consequently, measurements gave a velocity which was averaged over a fairly large region of the beam. Apparently, no attempt was made to determine the variation of velocity as a function of position or of operating conditions. Other than the previous reports concerning the axial velocities of ammonia MPD thruster exhausts and their relation to thruster performance by the authors of this report (refs. 3 and 4), only two other studies have been made - those by Malliaris and Libby (ref. 19) and by Kogelschatz (ref. 20). Malliaris and Libby measured the axial and rotational velocities of an ammonia MPD arc exhaust. The axial velocities were determined by using a chopping technique similar to that described in references 3 and 4. Unfortunately, they measured the velocities at only one axial position within 5 centimeters of the anode exit plane. Since the velocity strongly depends upon axial position and generally increases strongly beyond the anode exit plane, this could obscure a great deal of information. Furthermore, the results in reference 19 were obtained at fairly high tank pressures (0.01 to 0.1 torr). As shown earlier in this report and in reference 5, results obtained in this pressure range could differ considerably from those obtained at lower pressures. Furthermore, thrust and other thruster parameters were not measured. Consequently, we do not know if their thruster was operating the same as ours. However, in spite of these facts, their results are described briefly, as follows: In reference 19, neutral and ion axial velocities, as well as ion rotational velocities, were measured. No neutral rotational velocities were observed. Axial neutral velocities were at least an order of magnitude smaller than the ion velocities. Remarkably little dependence of axial velocity on arc power was found.

Our results can best be compared with those of Kogelschatz (ref. 20). He measured rotational and axial velocities at four axial positions, and found that the velocities increased with axial position, which is in agreement with our results. In addition, he noted that the ion rotational velocity decreased with axial position. This fact would illustrate that at least part of the thrust is obtained from the conversion of plasma rotation into directed energy in the magnetic nozzle. In reference 20, the axial neutral velocity was about 20 percent of the ion velocity, and there was no rotational motion of the neutrals.

A curious aspect of the results of Kogelschatz is the failure of the measured velocity to increase with increasing arc power. This is entirely inconsistent with the results of references 3 and 4 and with all our other measurements. The experiments of reference 20 seem very carefully done and are not easy to dismiss. We must therefore consider it probable that there are fundamental differences between the operation of the two different thrusters. Unfortunately, Kogelschatz did not make any supporting measurements of thruster operating parameters, such as thrust or thruster energy efficiency. It is not possible therefore to make a detailed comparison of thruster results. One indication that the thruster might be operating differently is the fact the N^{++} spectral lines are very intense in our beam, whereas Kogelschatz makes no mention of observing them.

ARC CURRENT DISTRIBUTION

There is a good deal of evidence that the arc current of MPD thrusters tends to concentrate into rotating spokes. (The rotating spoke was first noticed in a pulsed quasi-steady MPD arc by Lovberg (ref. 21). The first measurements showing a rotating spoke in a steady MPD arc were made by Larson (ref. 22).) Our Rogowski coil probe showed that such an arc current distribution exists in our ammonia thruster under a wide range of operating conditions with a rotational frequency in the hundreds of kilohertz range.

A typical oscilloscope trace of the integrated Rogowski coil output is shown in figure 21. Figure 22 shows the simultaneous integrated output of a pair of coils oriented 180° apart in the beam. This figure shows that the currents threading these two loops are approximately 180° out of phase, as would be expected for a rotating spoke.

The frequency of rotation of the current spoke in an ammonia arc is plotted as a function of mass flow rate in figure 23(a), of magnetic field strength in figure 23(b), and of arc current in figure 23(c). The frequency generally decreased with increasing mass flow rate and increased with increasing magnetic field or arc current. At mass flow rates above 0.05 gram per second, the detected signals became progressively smaller and less coherent with increasing flow rate. Similarly, at magnetic fields below 0.08 tesla, the signal became progressively smaller and less coherent with decreasing magnetic field. The signal disappeared entirely at a magnetic field of 0.05 tesla.

Data were obtained with the thruster operating in two voltage modes. The frequencies for both cases are shown in figure 23. Table II contains thruster operating data for the conditions for which frequencies are plotted in figure 23.

The thruster was also operated briefly on nitrogen and the beam probed with a Rogowski coil. For this study, the magnetic field was 0.1 tesla and mass flow rate was 0.15 gram per second. The arc current was varied from 550 to 1500 amperes. The Rogowski coil output is shown in figure 24 for a typical nitrogen data point. As before, a rotating current spoke is indicated. The oscilloscope trace for the point for which evidence of a rotating current spoke was not observed is shown in figure 25. Shortly after this observation was made, the arc voltage changed rather abruptly from 27 volts to about 32 volts. The next and all subsequent observations showed evidence of a rotating current spoke and an arc voltage above 30 volts. In summary then, the rotating current spoke was almost always present. It was not detected at very low magnetic fields and, in one case, for a low-voltage-mode run in nitrogen.

CONCLUDING REMARKS

A water-cooled magnetoplasmadynamic (MPD) arc thruster using ammonia propellant was studied to determine its performance capabilities and the factors upon which

performance depends. The thrust efficiency increased with increasing specific impulse or mass flow rate. The peak efficiency obtained was 25 percent at 2400 seconds specific impulse. Overall thruster performance was not appreciably affected by varying the magnetic field strength at constant power.

Studies of the energy and beam efficiencies, the exhaust velocities of propellant species, the spectral line intensities, and the arc voltage mode were made to determine the basic processes affecting thruster performance. With the high-voltage mode, anode losses were lower than for the low-voltage mode. This is primarily due to the fact that the thruster can be run at lower currents in this mode. However, the beam efficiency and spectroscopic studies showed that the fraction of ionization is higher in this mode and, consequently, the ionization losses are higher than in the low-voltage mode. In the low-voltage mode operation, the opposite is true; that is, due to the high currents necessary for equivalent power, the anode losses are high but the ionization losses are smaller.

Comparing the measured beam efficiencies with calculated frozen-flow efficiencies indicated that, in general, the plasma is partially ionized. This conclusion is supported by Doppler-shift measurements which show that there were fast neutrals, as well as ions, in the plasma exhaust. The neutral velocities were about equal to the ratio of thrust to mass flow rate, while the ion velocities were substantially higher. There is, of course, an inefficiency inherent in this ion slip.

The measurements also showed that the exhaust velocities increased sharply in the magnetic nozzle region outside the anode exit plane. This implies that a major portion of the thrust-producing mechanism is electromagnetic in nature.

The thruster performance was insensitive to magnetic field shape over a fairly wide range of field-shape parameter, including those given by optimum permanent-magnet designs.

The effect of tank pressure on thruster operation was studied by both thrust and spectroscopic measurements. Two competing effects were found. Background gas interfered with the normal thrust-producing mechanisms, reducing the exhaust velocity of the propellant. Background gas was also entrained and accelerated by the thruster. The net effect on measured thrust depended on mass flow rate and tank pressure.

For a wide range of operating conditions, the arc current was found to concentrate in the form of a rotating spoke. The frequency of rotation was in the hundreds of kilohertz range. It increased with increasing arc current or magnetic field or with decreasing mass flow rate.

Lewis Research Center,
National Aeronautics and Space Administration,
Cleveland, Ohio, March 16, 1970,
120-26.

REFERENCES

1. Johansen, Albert E.; and Palmer, Raymond W.: Lightweight Magnets for MPD Arcs. Paper 67-686, AIAA, Sept. 1967.

2. Connolly, Denis J.; Sovie, Ronald J.; Michels, Charles J.; and Burkhart, James A.: Low Environmental Pressure MPD Arc Tests. AIAA J., vol. 6, no. 7, July 1968, pp. 1271-1276.

3. Sovie, R. J.; and Connolly, D. J.: Doppler Measurements of the Exhaust Velocities in an MPD Thruster. Bull. Am. Phys. Soc., vol. 13, no. 11, Nov. 1968, p. 1513.

4. Sovie, R. J.; and Connolly, D. J.: A Study of the Axial Velocities in an Ammonia MPD Thruster. AIAA J., vol. 7, no. 4, Apr. 1969, pp. 723-725.

5. Connolly, D. J.; and Sovie, R. J.: The Effect of Background Pressure and Magnetic Field Shape on MPD Thruster Performance. Paper 69-243, AIAA, Mar. 1969.

6. Finke, Robert C.; Holmes, Arthur D.; and Keller, Thomas A.: Space Environment Facility for Electric Propulsion Systems Research. NASA TN D-2774, 1965.

7. John, R. R.; and Bennett, S.: Arcjet Technology Research and Development. Rep. RAD-SR-65-5, Arco Corp. (NASA CR-57452), Dec. 1964.

8. Jones, Robert E.; and Walker, Eddie L.: Status of Large Vacuum Facility Tests of MPD Arc Thrustor. Paper 66-117, AIAA, Jan. 1966.

9. Schneiderman, A. M.; and Patrick, R. M.: Optimization of the Thermal Efficiency of the Magnetic Annular Arc. Paper 66-115, AIAA, Jan. 1966.

10. Sovie, Ronald J.; and Klein, Barry M.: Volume Ion Production in a Tenuous Helium Plasma. NASA TN D-2324, 1964.

11. Dugan, John V., Jr.; and Sovie, Ronald J.: Volume Ion Production Costs in Tenuous Plasmas: A General Atom Theory and Detailed Results for Helium, Argon, and Cesium. NASA TN D-4150, 1967.

12. Nerheim, Noble M.; and Kelly, Arnold J.: A Critical Review of the Magnetoplasmadynamic (MPD) Thrustor for Space Applications. Rep. JPL-TR-32-1196, Jet Propulsion Lab, California Inst. Tech. (NASA CR-93139), Feb. 15, 1968.

13. Cann, G. L.; Harder, R. L.; Moore, R. A.; and Lenn, P. D.: Hall Current Accelerator. Rep. EOS-5470 - Final, Electro-Optical Systems, Inc. (NASA CR-54705), Feb. 4, 1966.

14. Cann, Gordon L.; Moore, Robert A.; Harder, Robert L.; and Jacobs, Paul F.: High Specific Impulse Thermal Arc Jet Thrustor Technology, Part II: Performance of Hall Arc Jets with Lithium Propellant. Rep. EOS-5090-Final, Electro-Optical Systems, Inc. (AFAPL-TR-65-48, pt. 2, DDC No. AD-805309), Jan. 1967.

15. Sovie, Ronald J.: Spectroscopic Determination of Electron Temperature and Percentage Ionization in a Helium Plasma. Phys. Fluids, vol. 7, no. 4, Apr. 1964, pp. 613-614.

16. Sovie, R. J.: The Effects of Cascading and Metastable Atoms on the Determination of Electron Temperature from Relative Line Intensities in a Tenuous Helium Plasma. J. Quant. Spectrosc. Radiat. Transfer, vol. 8, no. 2, Feb. 1968, pp. 833-838.

17. Bohn, W. L.; Beth, M.-U.; and Nedder, G.: On Spectroscopic Measurements of Velocity Profiles and Non-Equilibrium Radial Temperatures in an Argon Plasma Jet. J. Quant. Spectrosc. Radiat. Transfer, vol. 7, no. 4, 1967, pp. 661-676.

18. Jacobs, P. F.; Cann, G. L.; and Harder, R. L.: Diagnostic Measurements in Alpha (Alkali Plasma Hall Accelerator). Rep. EOS-7053-Final, Electro-Optical Systems, Inc. (NASA CR-72233), May 31, 1967.

19. Malliaris, A. C.; and Libby, D. R.: Velocities of Neutral and Ionic Species in an MPD Flow. Paper 69-109, AIAA, Jan. 1969.

20. Kogelschatz, Ulrich: Doppler-Shift Measurements of Axial and Rotational Velocities in an MPD Arc. Paper 69-110, AIAA, Jan. 1969.

21. Lovberg, R. H.: Physical Processes in the Magneto-Plasmadynamic Arc. California Univ. (NASA CR-83891), Mar. 1967.

22. Larson, A. V.: Experiments on Current Rotations in an MPD Engine. AIAA J., vol. 6, no. 6, June 1968, pp. 1001-1006.

TABLE I. - SPECTRAL LINES MONITORED FOR EACH ELEMENT

Element						
N	N^+	N^{++}	H	H_2	N_2	N_2^+
Wavelength of spectral lines, Å						
4100	4643.1	4634.1	4861.3	4069.6	Second positive system bands at 3576.9 and 3536.7	First negative system bands at 3914.1, 3582.1, and 3563.9
4110	4631.1	4103.4	4107.7	4066.9		
	4621.6	4097.3		4062.5		
	4073					
	3919					

TABLE II. - MAGNETOPLASMADYNAMIC (MPD) ARC DATA

Run	Magnetic field, B, T	Arc current, I_a, A	Arc voltage, V_a, V	Arc power, P_a, kW	Anode loss, P_{an}, kW	Cathode loss, P_{cat}, kW	Thermal efficiency, η_{th}, percent	Spoke frequency, f_{sp}, kHz	Arc chamber pressure, P_c, torr	Propellant flow rate, $\dot{m}$, g/sec
1	0.10	500	51	25.5	12.7	0.6	48	255	20.4	0.06
2	↓	↓	50	25.0	12.6	.6	47	280	17.7	.05
3	↓	↓	49	24.5	13.1	.7	44	319	14.9	.04
4	↓	↓	48	24.0	13.1	.7	42	368	11.6	.03
5	↓	↓	52	26.0	14.1	.7	43	409	8.4	.02
6	↓	↓	54	27.0	14.8	.8	42	480	6.9	.015
7	↓	200	57	11.4	6.2	.5	41	194	8.5	.03
8	↓	300	51	15.3	7.9	.6	44	270	9.7	↓
9	↓	400	48	19.2	10.5	.7	42	326	10.8	↓
10	↓	500	46	23.0	12.6	.8	42	358	11.5	↓
11	↓	600	44	26.4	15.1	.9	39	356	12.5	↓
12	↓	700	42	29.4	17.4	1.0	37	355	13.3	↓
13	↓	800	41	32.8	20.0	↓	36	367	13.8	↓
14	↓	900	40	36.0	22.3	↓	35	374	14.2	↓
15	.07	500	41	20.5	12.1	↓	36	238	12.8	↓
16	.08	↓	43	21.5	12.6	.9	37	295	12.4	↓
17	.10	↓	50	25.0	13.9	.9	41	361	11.6	↓
18	.12	↓	59	29.5	15.3	.8	45	426	11.5	↓
19	.14	↓	64	32.0	16.3	.8	47	484	11.7	↓
20	.16	↓	68	34.0	16.8	.8	48	521	12.3	↓
21	.1	↓	59	29.5	15.2	1.0	45	270	21.9	0.06
22	↓	↓	60	30.0	15.4	1.1	45	276	18.8	.05
23	↓	↓	59	29.5	15.4	1.1	44	290	15.6	.04
24	↓	↓	57	28.5	15.0	1.2	43	338	12.1	.03
25	↓	↓	59	29.5	15.4	1.2	44	415	8.8	.02
26	↓	↓	60	30.0	16.0	1.2	43	489	7.1	.015
27	↓	↓	57	28.5	15.0	1.1	43	347	11.9	.03
28	↓	210	63	13.7	6.7	.9	42	135	9.0	↓
29	↓	300	61	18.3	9.6	1.0	42	233	10.5	↓
30	↓	400	59	23.6	12.1	1.1	44	278	11.3	↓
31	↓	500	57	28.5	15.0	1.1	43	336	12.1	↓
32	↓	600	56	33.6	17.9	1.2	43	377	12.5	↓
33	↓	700	55	38.5	20.7	1.3	43	419	12.8	↓
34	↓	800	↓	44.0	24.6	1.3	41	460	12.7	↓
35	↓	900	↓	49.5	26.9	1.4	43	498	12.6	↓
36	↓	1000	↓	55.0	30.9	1.4	41	465	12.5	↓
37	.07	500	61	30.5	15.4	1.2	46	---	13.8	↓
38	.08	↓	58	29.0	15.4	1.2	43	235	13.1	↓
39	.1	↓	56	28.0	15.0	1.2	42	333	12.2	↓
40	.12	↓	60	30.0	15.4	1.1	45	400	11.8	↓
41	.14	↓	65	32.5	16.4	1.1	46	470	11.9	↓

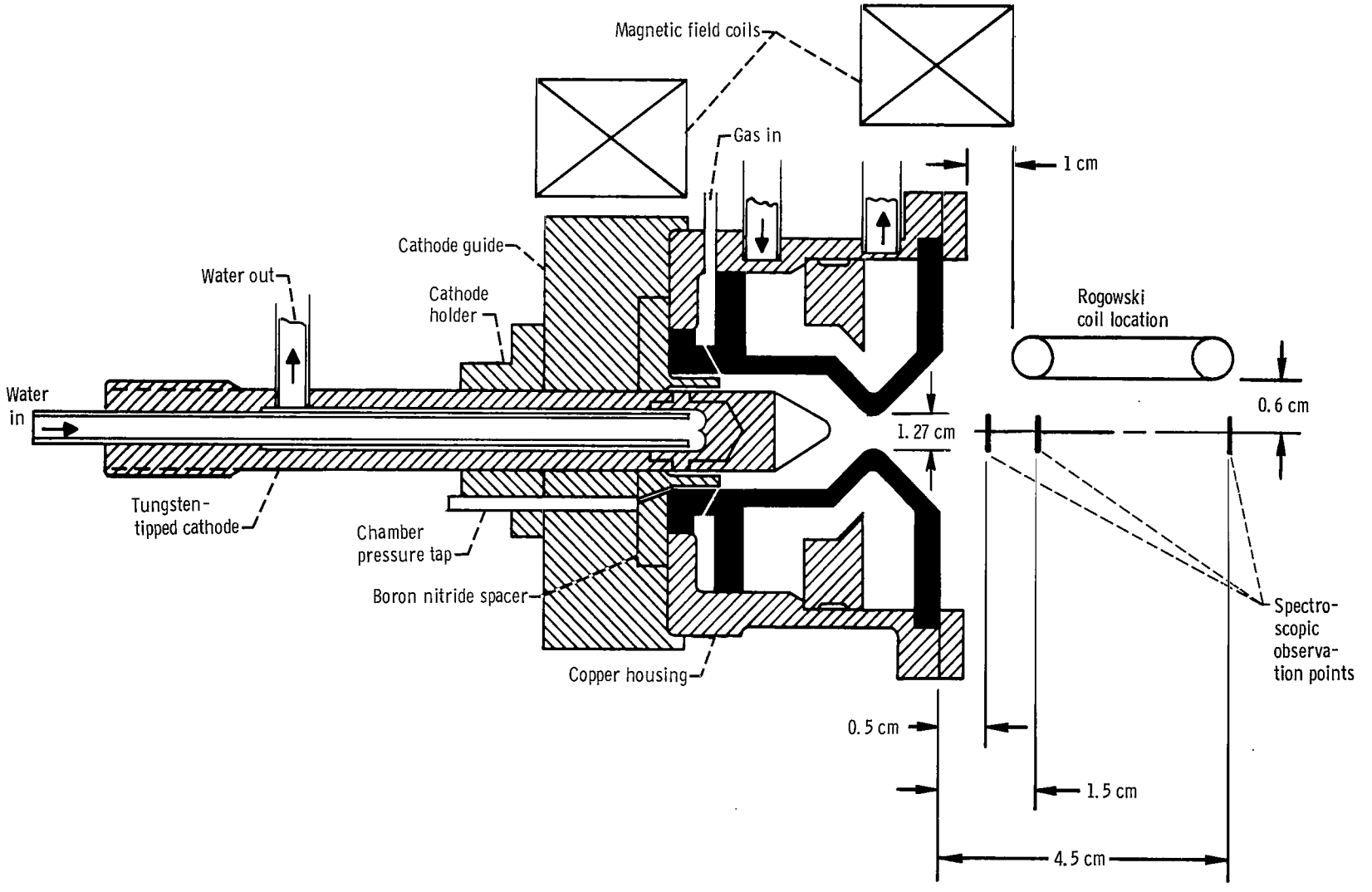

Figure 1. - Schematic of water-cooled magnetoplasmadynamic (MPD) arc thruster.

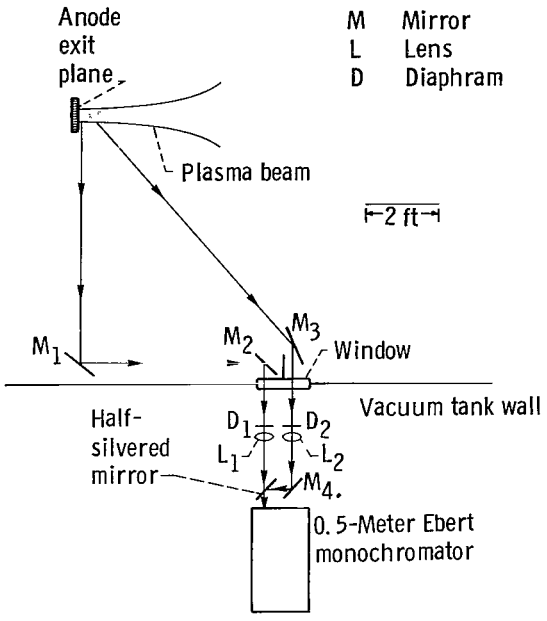

Figure 2. - Optical arrangement.

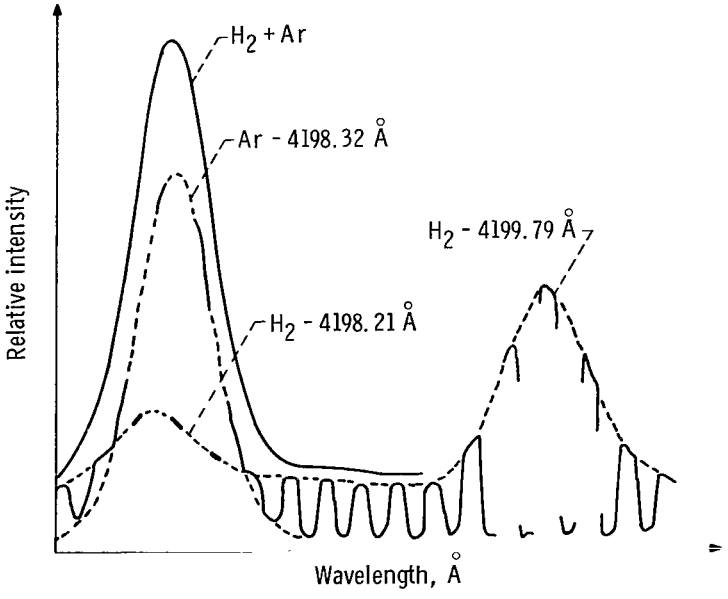

Figure 3. - Monochromator spectral line traces.

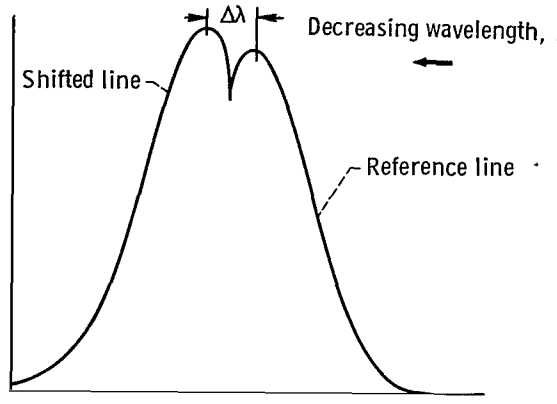

(a) Nitrogen ions; wavelength, λ = 4631 Å; shift in wavelength, $\Delta\lambda$ = 0.172 Å.

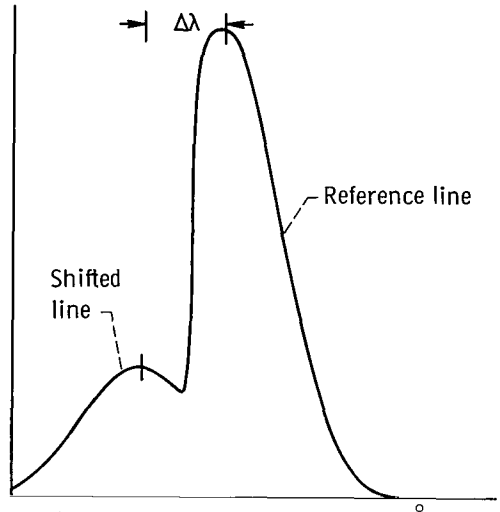

(b) Nitrogen ions; wavelength, λ = 4631 Å; shift in wavelength, $\Delta\lambda$ = 0.265 Å.

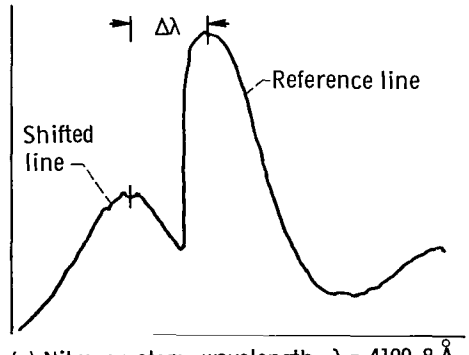

(c) Nitrogen atom; wavelength, λ = 4109.8 Å; shift in wavelength, $\Delta\lambda$ = 0.26 Å.

Figure 4. - Reproduction of actual data traces obtained using a single chop.

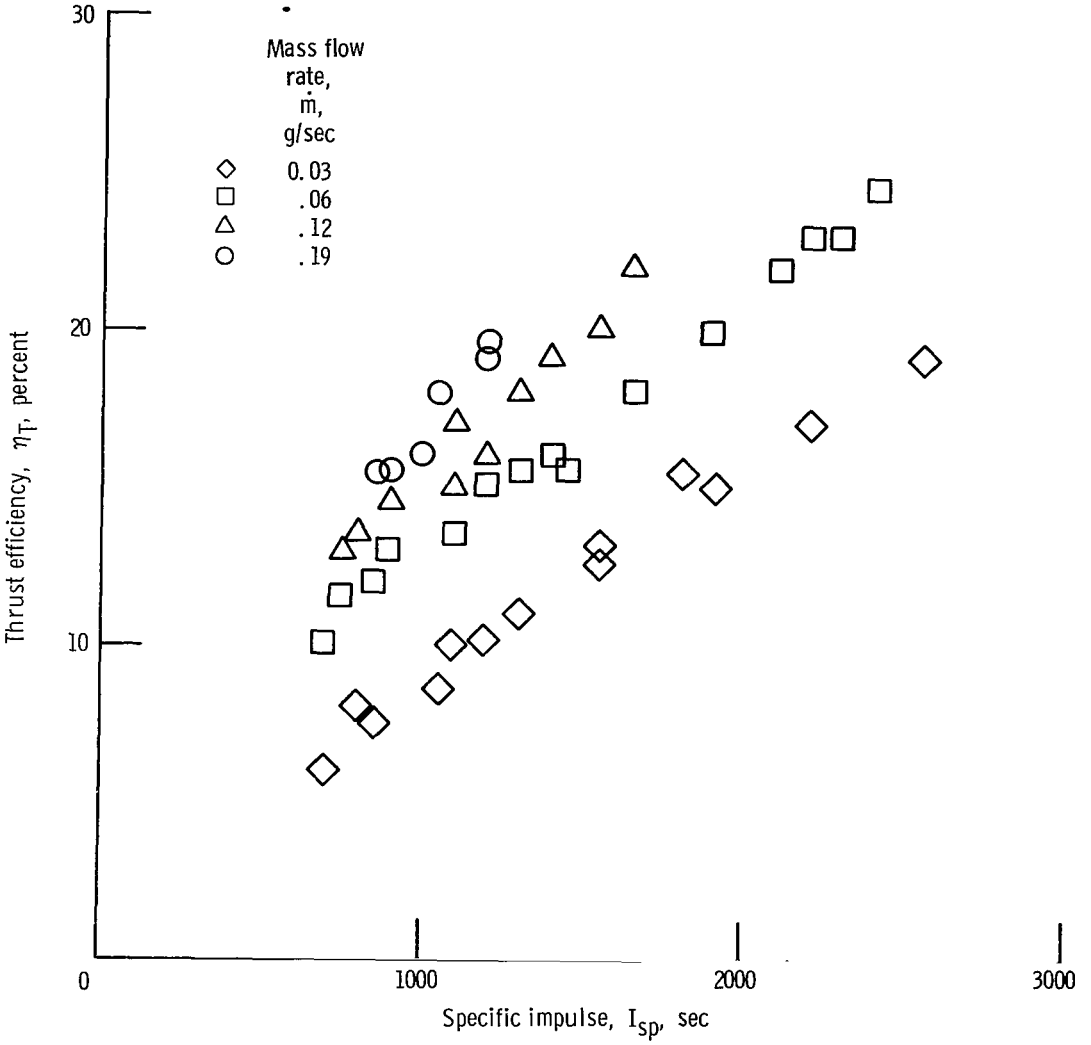

Figure 5. - Thrust efficiency against specific impulse for ammonia propellant.

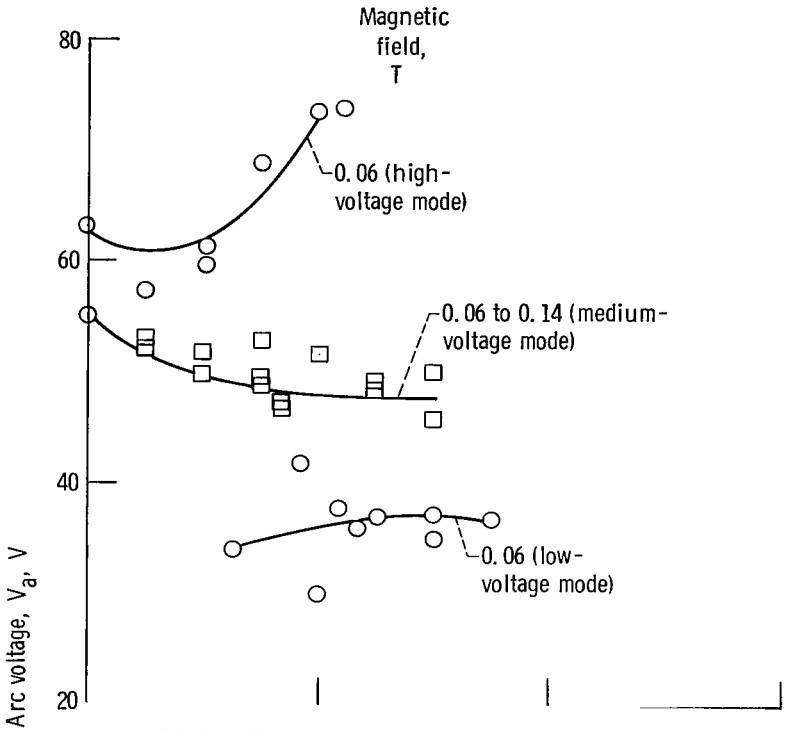

(a) Mass flow rates, 0.02 and 0.03 gram per second.

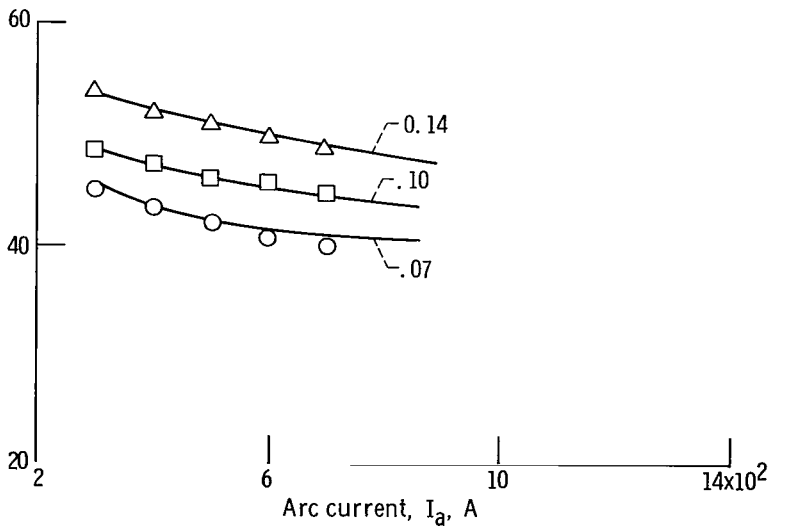

(b) Mass flow rate, 0.06 gram per second.

Figure 6. - Arc voltage-current characteristic for ammonia arc.

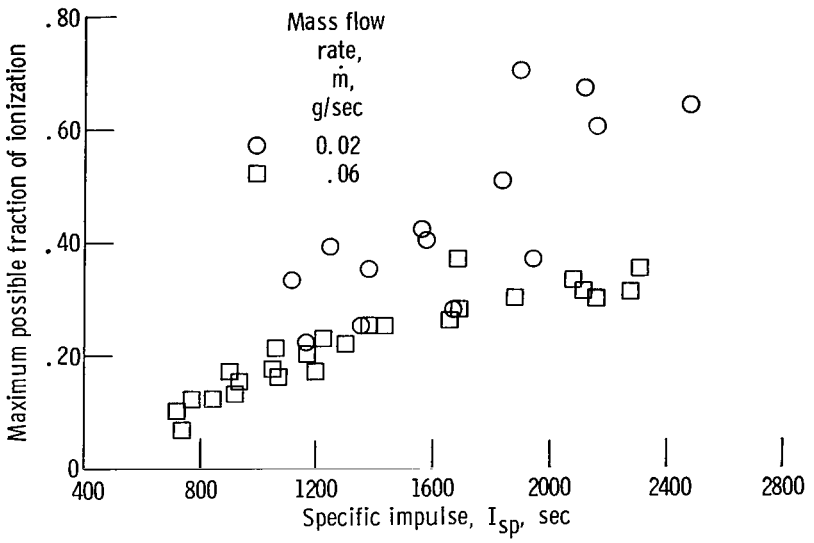

Figure 7. - Maximum fraction of ionization against specific impulse for ammonia propellant.

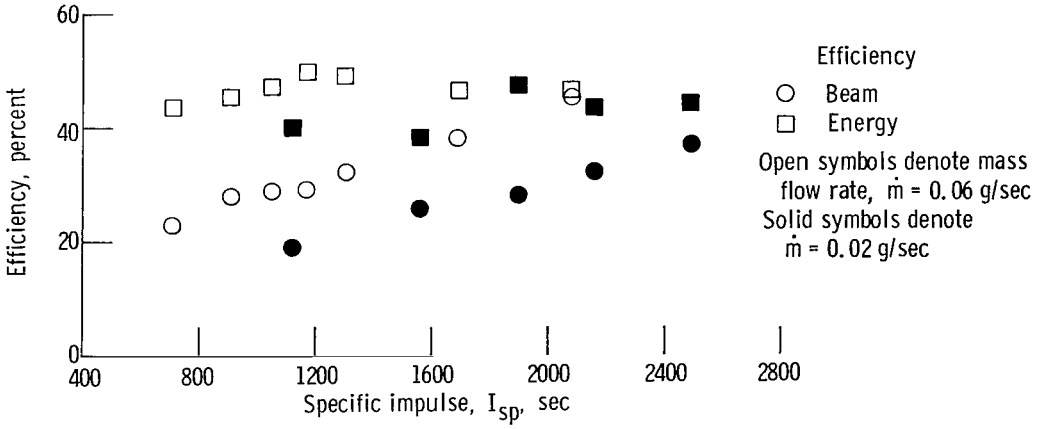

Figure 8. - Energy and beam efficiencies against specific impulse for ammonia propellant.

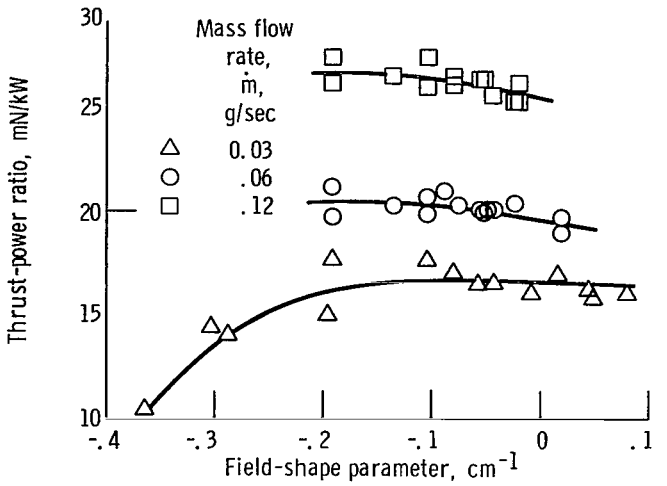

Figure 9. - Thrust-to-arc-power ratio against field-shape parameter for ammonia propellant.

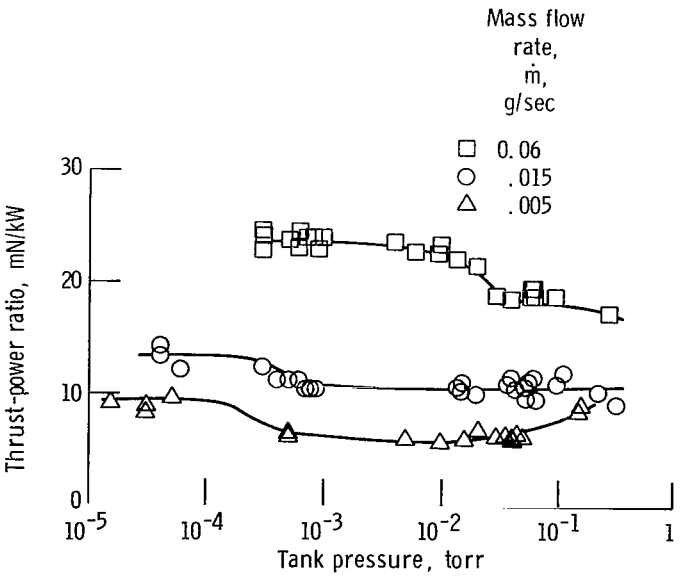

Figure 10. - Thrust-to-arc-power ratio against tank pressure for ammonia propellant.

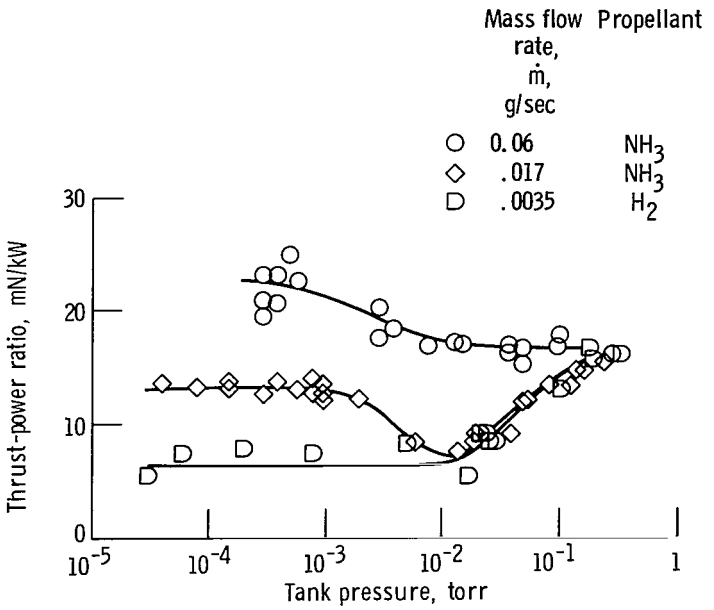

Figure 11. - Thrust-to-arc-power ratio against tank pressure for nitrogen background.

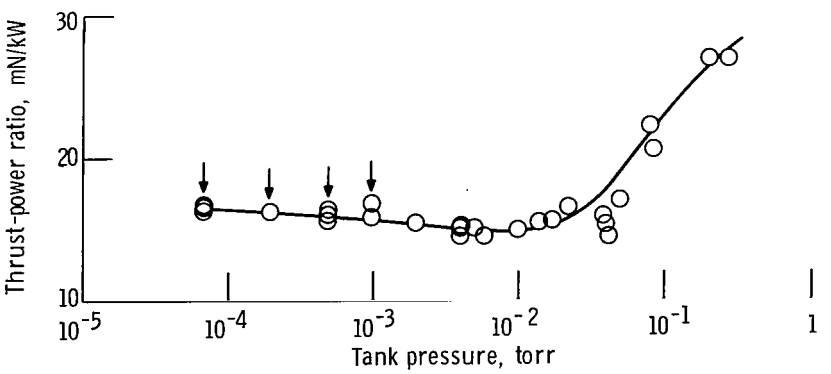

Figure 12. - Thrust-to-arc-power ratio against tank pressure for ammonia propellant and argon background gas. (Arrows indicate the tank pressures for which axial velocity is plotted against axial position in fig. 13.)

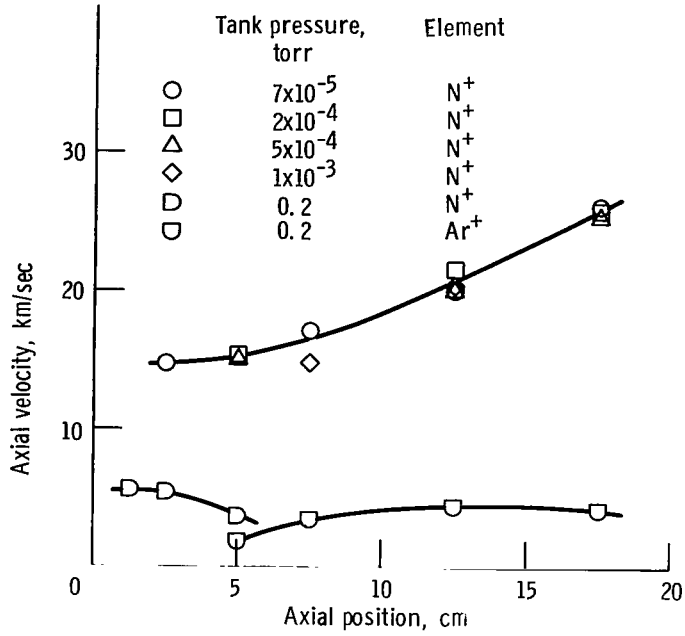

Figure 13. - Axial velocity against axial position for singly ionized nitrogen atom. Ammonia propellant; argon background.

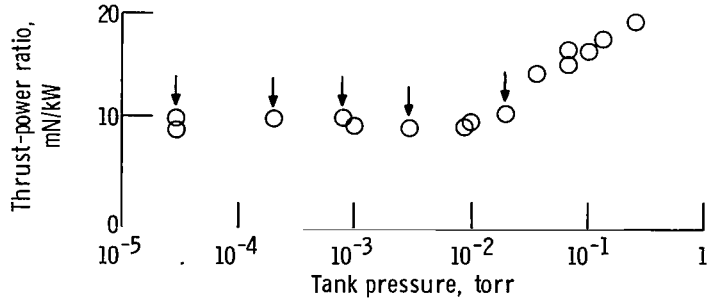

Figure 14. - Thrust-to-arc-power ratio against tank pressure for hydrogen propellant and nitrogen background gas. (Arrows indicate tank pressures at which spectroscopic data were taken.)

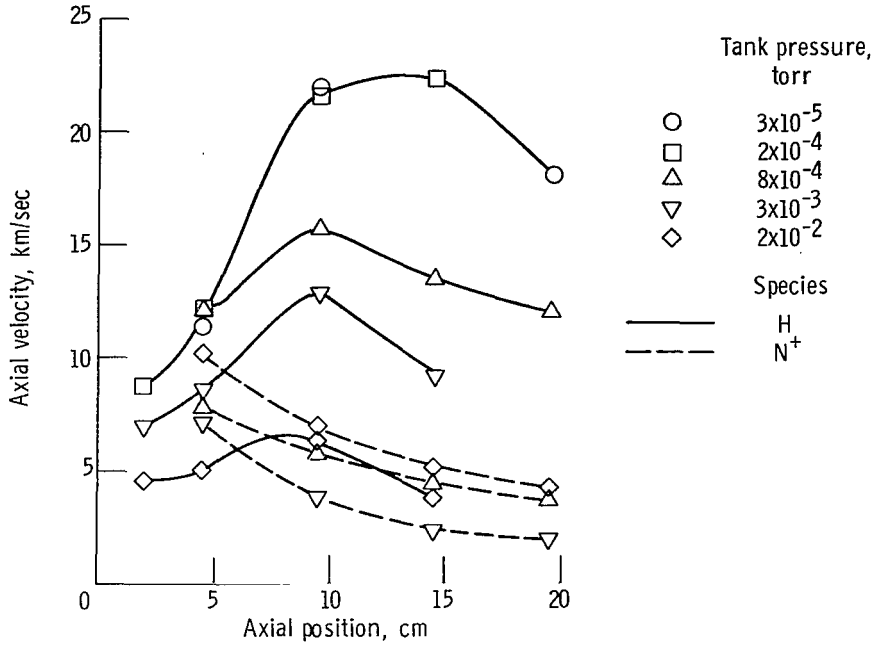

Figure 15. - Axial velocity against axial position for hydrogen propellant and nitrogen background.

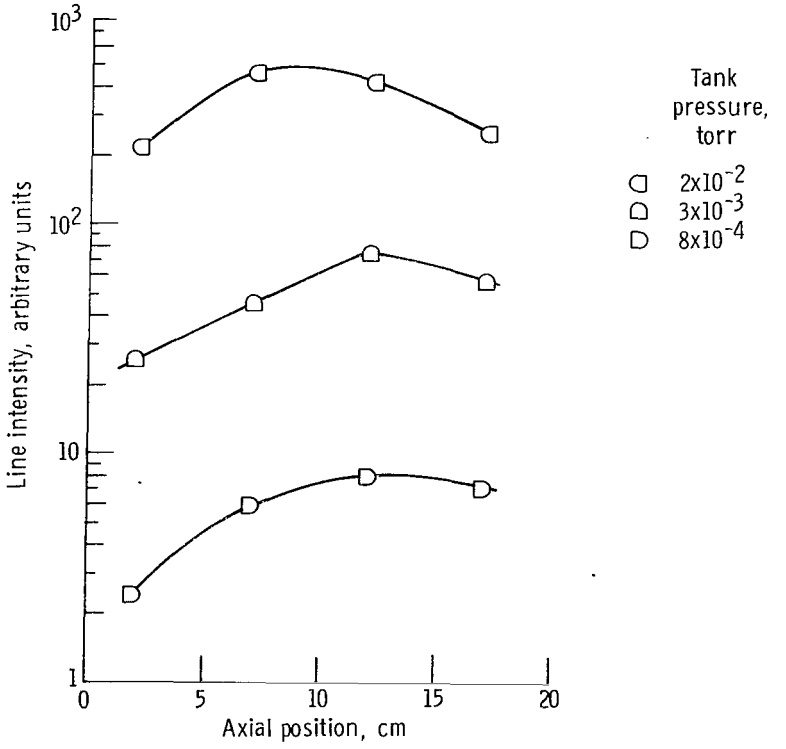

Figure 16. - Nitrogen ion line intensity against axial position for hydrogen propellant and nitrogen background.

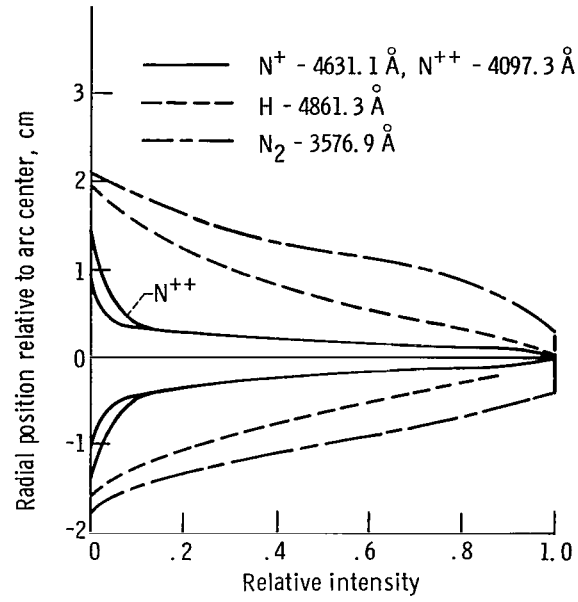

Figure 17. - Radial variation of integrated spectral line intensities in ammonia, 0.5 centimeter downstream of exit plane of anode.

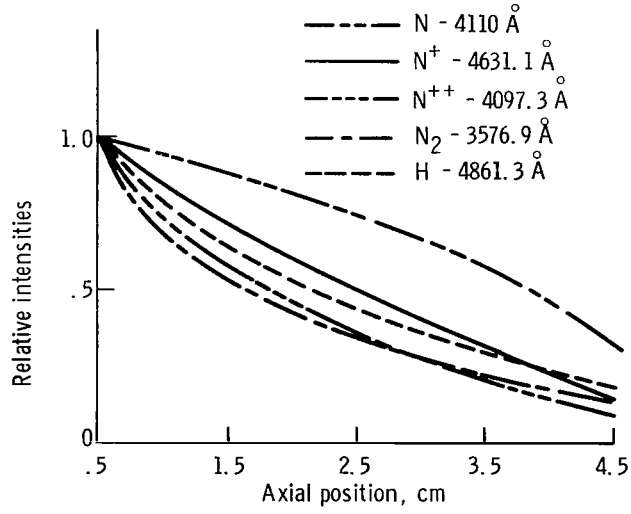

Figure 18. - Axial variation of line intensities.

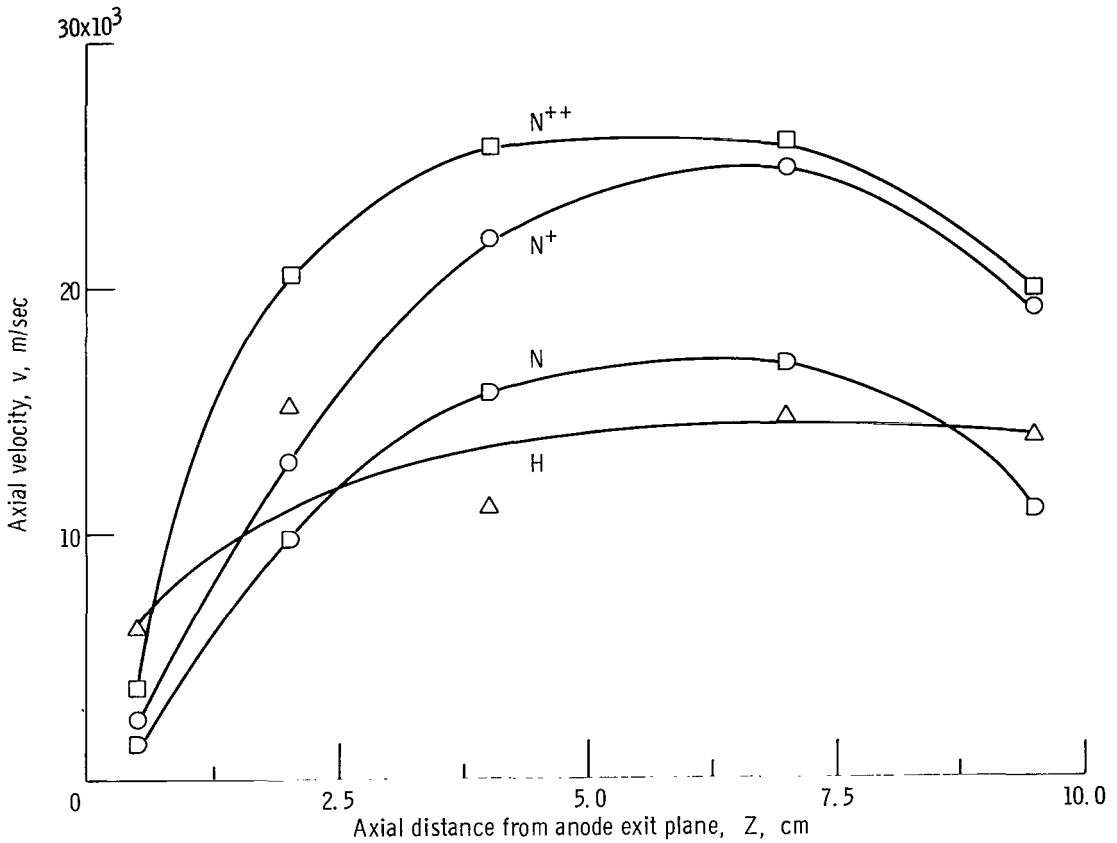

Figure 19. - Typical values of axial velocity against axial distance. Magnetic field, 0.1 tesla; mass flow rate, 0.02 gram per second; arc voltage, 52.5 volts; specific impulse, 1765 seconds; and thrust efficiency, 10 percent.

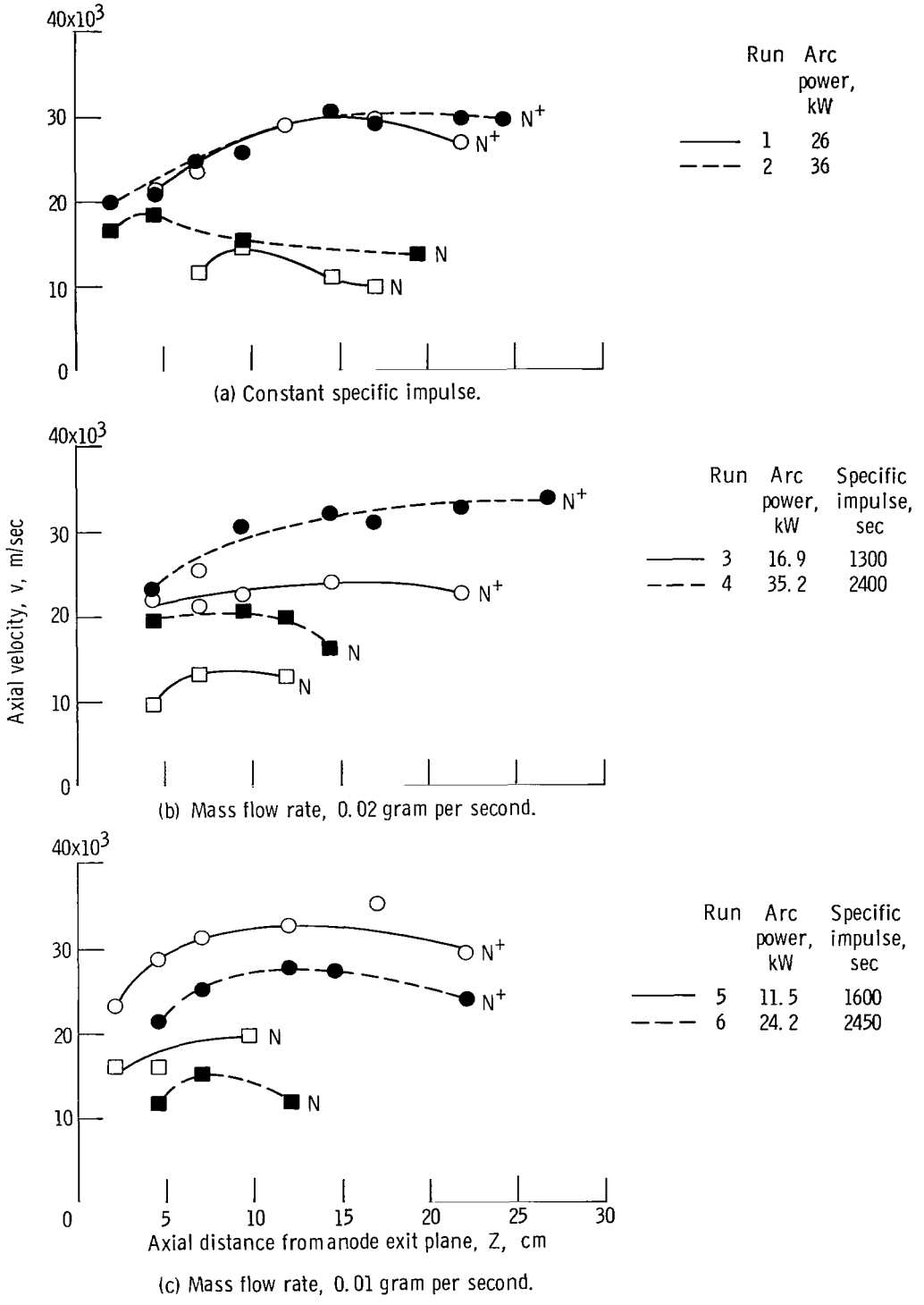

Figure 20. - Axial velocity against axial distance from anode exit plane for constant values of specific impulse and mass flow rate. Magnetic field, 0.15 tesla.

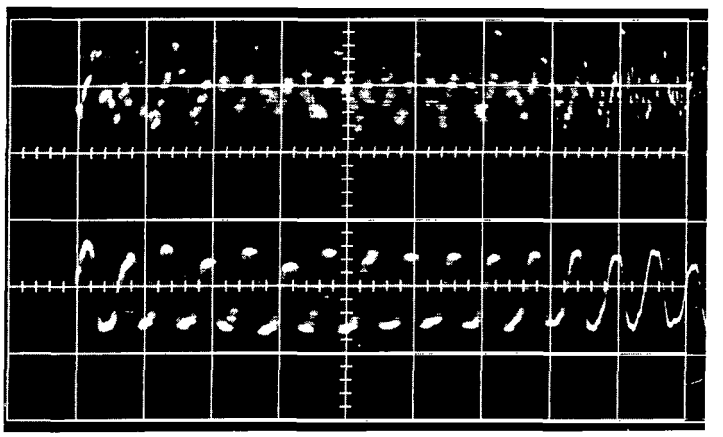

Figure 21. - Rogowski coil signal for ammonia propellant. Sweep speed, 5 microseconds per centimeter; vertical sensitivity, 0.95 ampere per centimeter. Thruster conditions: magnetic field, 0.14 tesla; arc current, 400 amperes; flow rate, 0.03 gram per second. Upper trace is unintegrated coil output; lower trace is integrated signal (inverted).

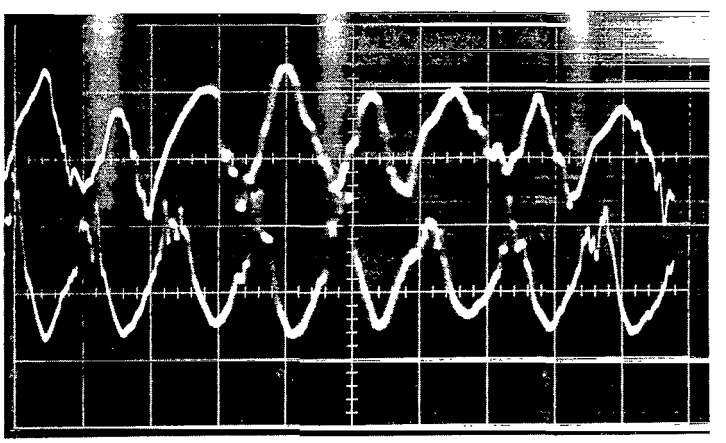

Figure 22. - Output of Rogowski coil pair arranged diametrically across beam. Sweep speed, 2 microseconds per centimeter; vertical sensitivity, 3.3 amperes per centimeter. Thruster conditions: magnetic field, 0.1 tesla; arc current, 640 amperes; flow rate, 0.02 gram per second.

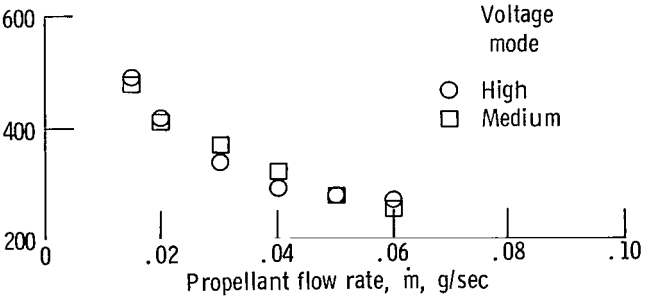

(a) Arc current, 500 amperes; magnetic field, 0.10 tesla.

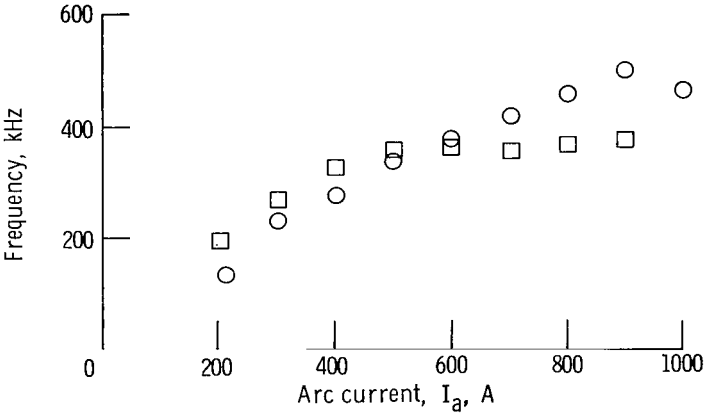

(b) Magnetic field, 0.10 tesla; flow rate, 0.03 gram per second.

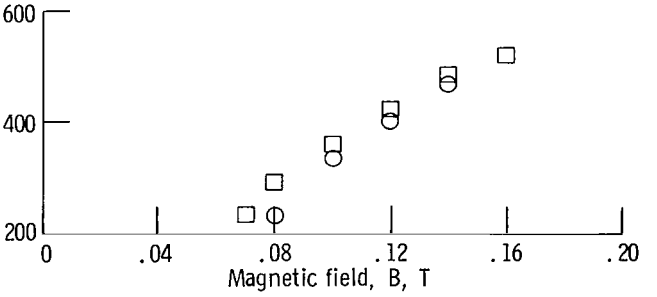

(c) Arc current, 500 amperes; flow rate, 0.03 gram per second.

Figure 23. - Frequency of rotation against propellant flow rate, arc current, and magnetic field.

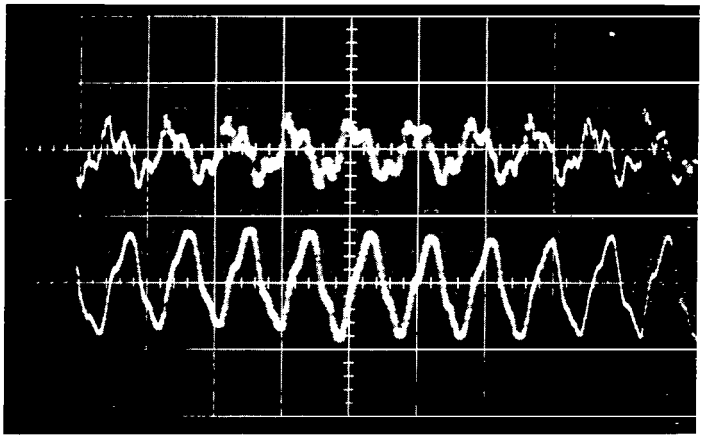

Figure 24. - Rogowski coil output for N_2 propellant. Sweep speed, 5 microseconds per centimeter; vertical sensitivity, 2.8 amperes per centimeter; flow rate, 0.15 gram per second; magnetic field, 0.10 tesla; arc current, 1500 amperes; arc voltage, 33 volts.

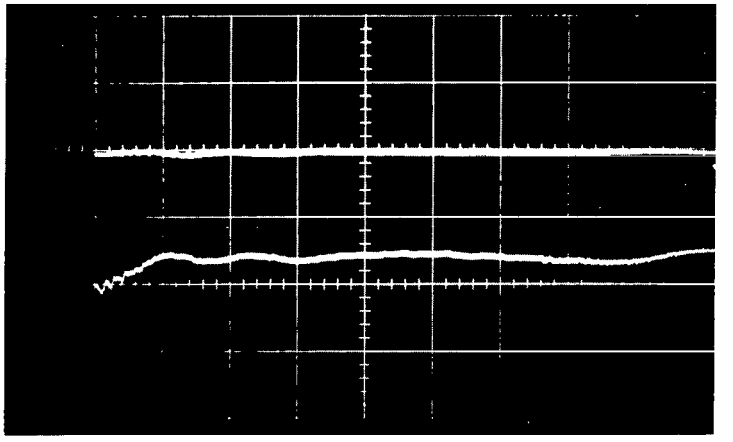

Figure 25. - Rogowski coil output for N_2 propellant. Sweep speed, 5 microseconds per centimeter; vertical sensitivity, 2.8 amperes per centimeter; flow rate, 0.15 gram per second; magnetic field, 0.10 tesla; arc current, 750 amperes; arc voltage, 27 volts.

NASA-Langley, 1970 —— 28 E-5561